ELSEVIER

Journal of Structural Geology 29 (2007) 141–158

JOURNAL OF STRUCTURAL GEOLOGY

www.elsevier.com/locate/jsg

Deformation patterns and structural vergence in brittle–ductile thrust wedges: An additional analogue modelling perspective

Marco Bonini*

Consiglio Nazionale delle Ricerche (CNR), Istituto di Geoscienze e Georisorse (IGG), Via G. La Pira 4, I-50121 Firenze, Italy

Received 3 November 2005; received in revised form 26 May 2006; accepted 21 June 2006
Available online 9 October 2006

Abstract

Scaled physical models of brittle–ductile thrust wedges investigated the causes leading to the development of the various structural styles observed in fold-and-thrust belts and accretionary prisms. This study focused on some potential controlling factors, such as (1) relative strength between the brittle overburden and the viscous décollement layer (brittle–ductile coupling), (2) the effect of very low basal friction, and (3) pre-shortening rheological stratigraphy, including décollement strength. Type 1 models had a single basal décollement, whereas in Type 2 models the décollement was embedded in brittle material simulating an upper roof sequence and a lower floor sequence. Other models investigated the effects produced by an horizon of mechanical weakness at the base of the viscous décollement (Type 1a), and the role of décollement offset (Type 3). The experiments suggest the occurrence of a genetic relationship between the absolute values of shear stresses and the development of dominating hinterland- or foreland-verging thrust faults, or dually-verging thrusts. By controlling the orientation of the σ_1 axis, basal friction and décollement offset is found to effectively influence the deformation pattern and structural vergence, and could explain the development of dominating backthrusts in Cascadian-type margins. The decoupling of a frontal monocline via the upper décollement (Type 2 models) produced passive-roof duplex structures, termed ''composite-roof duplex'' when the frontal monocline coexists with outward fold propagation.

Keywords: Analogue modelling; Brittle–ductile thrust wedges; Thrust polarity; Passive-roof duplexes

1. Introduction

Fold-and-thrust belts and their submarine equivalent accretionary wedges are composed of thrust faults depicting a general forelandward vergence, but hinterland-verging or dually-verging thrusts may dominate as well. The main structural vergence of fold-and-thrust belts is essentially controlled by the orientation of the principal stress σ_1 axis, which determines which set of the conjugate thrust fault pair will predominate. The control of basal friction on the development of either foreland or hinterland vergent thrusts has been elegantly exemplified by Davis and Engelder (1985) (Fig. 1a). High basal friction will result in a regional σ_1 axis dipping toward the foreland (Hafner, 1951; Chapple, 1978; Mandl and Shippam, 1981), so that foreland-verging thrusts will dip more gently than the conjugate (hinterland verging) thrusts (Fig. 1b). The former thrust set will be thus favoured as a shallower dip allows to accommodate a greater amount of horizontal shortening for the same increase in gravitational potential energy (Davis and Engelder, 1985). The presence of a basal décollement is expected to favour a nearly horizontal σ_1 axis (Chapple, 1978), such that a dual vergence will be favoured (Davis and Engelder, 1985), as is the case of some fold-and-thrust belts detached above a single ductile layer (Fig. 1c). In spite of this prediction, several fold-and-thrust belts detaching above a décollement display a dominant foreland vergence (Fig. 1d), thus suggesting that thrust wedge deformation may be governed by additional factors.

* Tel.: +39 055 2757528; fax: +39 055 290312.
E-mail address: mbonini@geo.unifi.it

0191-8141/$ - see front matter © 2006 Elsevier Ltd. All rights reserved.
doi:10.1016/j.jsg.2006.06.012

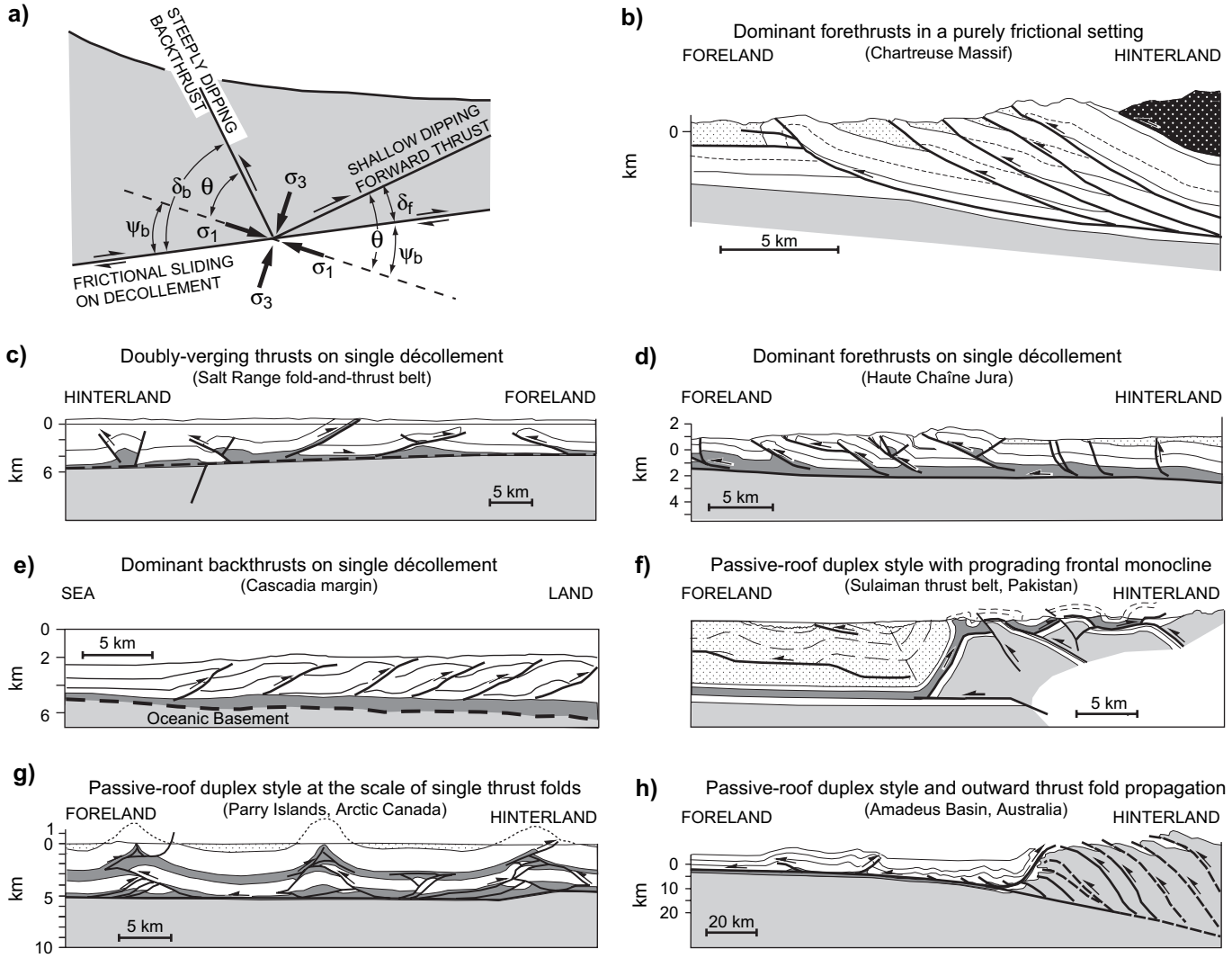

Fig. 1. (a) Relations between principal stress axes and conjugate thrust faults (after Davis and Engelder, 1985). Main structural patterns in fold-and-thrust belts and accretionary prisms: (b) Chartreuse Massif (after Philippe, 1995 in Jouanne et al., 1998), (c) Salt Range fold-and-thrust belt (after Pennock et al., 1989), (d) Haute Chaîne Jura (after Sommaruga, 1999), (e) Cascadia margin (after Gutscher et al., 2001), (f) Sulaiman thrust belt, Pakistan (after Banks and Warburton, 1986), (g) Parry Islands, Arctic Canada (after Harrison, 1995), (h) Amadeus Basin, Australia (after Teyssier, 1985).

Hinterland-verging thrusts may be either dominating, or, most commonly, develop in close association with ''normal'' foreland-verging thrusts. Dominating backthrusts (i.e., landward) have been mostly documented in the Oregon–Cascadia accretionary prism (Dickinson and Seely, 1979; McKay et al., 1992; MacKay, 1995; Fig. 1e). On the contrary, dually-verging thrusts have been described worldwide. Because of their variable geometric/kinematic setting, thrust triangle zones have been referred to various models (see Mackay et al., 1996 and Barnes and Nicol, 2004, for a review). These may be broadly subdivided into (1) opposite-verging thrusts, when detaching above a single décollement, and (2) passive-roof duplex (or tectonic wedge) structures, when developing in a multilayer system consisting of (at least) an upper décollement in addition to the basal one. Passive-roof duplexes (Banks and Warburton, 1986) have been frequently identified at the deformation front of fold-and-thrust belts (Gordy et al., 1977; Price, 1981; Fig. 1f, h). However, these structures, owing to their scale-invariance, may also develop in the interior of a growing thrust belt, as well as at the scale of a single thrust fold (e.g., De Feyter and Menichetti, 1986; Harrison, 1995; Mueller and Suppe, 1997; Couzens-Schultz et al., 2003; Fig. 1g).

The factors leading to the above structural styles have been widely investigated by means of different modelling approaches – i.e., analytical (e.g., Elliott, 1976; Chapple, 1978; Mandl and Shippam, 1981; Davis et al., 1983), numerical (e.g., Willett et al., 1993; Erickson, 1995; Strayer et al., 2001; Salvini et al., 2001; Wissing et al., 2003; Ellis et al., 2004), and analogue (e.g., Mulugeta and Koyi, 1987; Colletta et al., 1991; Cobbold et al., 1995; Gutscher et al., 1998; Koyi et al., 2000). In this work, a series of laboratory experiments on brittle–ductile thrust wedge (non-Coulomb wedges) is used to study in more detail the effects of varying initial conditions on the resulting deformation patterns. The present work intends to test and to explore some factors that are potentially able to control the structural style and thrust vergence of

brittle–ductile thrust wedges and accretionary complexes. The factors under investigation, which will be addressed in more detail in the following Section 2.1, are connected with: (1) relative strength of the brittle overburden and décollement (brittle–ductile coupling), (2) very low basal friction and its effect on the orientation of the σ_1 axis, and (3) pre-shortening rheological stratigraphy, including initial décollement strength.

A broad spectrum of thrusting patterns is obtained, varying from dominating forethrusts or backthrusts, to systems showing a dual vergence with a clear sequence of thrusting. Stress analysis shows that the various thrusting patterns may result from variations in the mechanical coupling between brittle and ductile layers, as well as from pre-shortening rheological conditions. Modelling results are then compared with field examples from the Apennines.

2. Analogue modelling

2.1. Modelling strategy

The controlling factors of thrust wedge deformation considered in the present experimental study are discussed below separately.

2.1.1. Brittle–ductile coupling (Type 1 models)

Previous experimental work on continental extension has demonstrated that the deformation style is strongly dependent upon the coupling between brittle and ductile layers. This latter can be expressed by the ratio of brittle strength to ductile strength (Allemand, 1988), which is equivalent to the dimensionless ratio χ of décollement strength to wedge strength in fold-and-thrust belts (Chapple, 1978; Stockmal, 1983).

The results of recent analogue models considering a brittle overburden detached above a single décollement layer point to the importance of décollement strength and brittle–ductile coupling as controlling factors of thrust wedges deformation (Gutscher et al., 2001; Costa and Vendeville, 2002; Smit et al., 2003). However, they imply partly different conclusions about the relations between brittle–ductile coupling and thrust polarity. For instance, distinct deformation styles (i.e., dominant forethrusts, backthrusts, dually-verging thrusts) are linked to specific ranges of strain rates in the models by Gutscher et al. (2001). In comparison, the thrust wedges in Smit et al. (2003) consisted of compartments showing dominant forethrusts backthrusts – thereby an essential dual vergence – for a large spectrum of brittle–ductile coupling. This apparent discrepancy may be, however, possibly due to an incomplete view of the relations between brittle–ductile coupling and thrust wedge deformation. A same brittle–ductile shear stress ratio can indeed result from various combinations among the different factors influencing brittle and ductile strength (i.e., pore fluid pressure, strain rate, décollement viscosity, overburden and décollement thickness). Consequently, a given brittle–ductile shear stress ratio may not necessarily correspond to a specific deformation pattern. This aspect has been here examined in more detail by considering a broader field of brittle–ductile coupling in a series of Type 1 models shortened above a single décollement. This goal has been achieved by introducing extreme variations in décollement strength coupled with a systematic variation in overburden thickness (i.e., strength). Thus, Type 1 model set-up has allowed to investigate an extensive range of brittle–ductile stress ratios (τ_b/τ_d), varying from ca. 1.2 to 743 (see τ_b and τ_d values in Table 1; for comparison, such ratios are $\leq$350 in Smit et al., 2003).

2.1.2. Low basal friction (Type 1a models)

Previous analogue modelling has shown that basal friction is fundamental in controlling the structural vergence as well as the sense and amount of thrust propagation (Mulugeta, 1988; Vendeville, 1991; Koyi et al., 2000; Nieuwland et al., 2000; Costa and Vendeville, 2002; Massoli et al., 2006). Very low friction is obviously influenced by the physical conditions of the décollement layer. Specifically, the presence of a very weak horizon at the base of the décollement may affect the transmission of stresses and then the bulk shear within this layer. Mechanical zones of weakness may arise from the localization of overpressured fluids, or from internal sedimentary variations (such as differentiation of salt and anhydrite). These factors are expected to potentially influence the overall sense of shearing along the décollement layer. Basal shear is able, in turn, to control the rotation and orientation of the σ_1 axis (e.g., Gartrell, 2001). The current modelling has addressed this clue by performing a set of models (Type 1a) investigating the role that an horizon of mechanical weakness at the base of the viscous décollement may exert on the structural outcome, including the development of diapiric processes at the core of detachment folds (hybrid Type 1a models).

2.1.3. Pre-shortening rheological stratigraphy (Types 2 and 3 models)

The relevance of the initial rheological layering is exemplified by the comparison between Type 1 models with previous models (reported in Bonini, 2001, 2003, and referred to here as Type 2) in which the rheological stratigraphy consisted of a ductile layer embedded between an overlying brittle roof sequence and an underlying brittle floor sequence. In Type 2 models, brittle–ductile coupling was varied over a wide range of combination of brittle and ductile strengths (shear stress ratios varying from ca. 0.5 to 83) by varying (1) the roof sequence/décollement thickness ratio (H_b/H_d), and (2) the strain rate in the décollement.

Finally, brittle–ductile models applied to the Salt Range in Pakistan (Cotton and Koyi, 2000) suggest that a lateral rheological contrast may also provide a key for understanding the occurrence of dominating hinterland-verging structures. In this respect, a few test models (Type 3 models) investigated how the structural style of thrust wedges may be affected by a lateral rheological contrast arising from fault offset.

2.2. Model construction and deformation

The modelling procedure was performed at the Tectonic Modelling Laboratory of the CNR – Istituto di Geoscienze

Table 1
Analogue models parameters

Model	H_b (cm)	H_d (cm)	v (cm h^{-1})	τ_b (Pa)	τ_d (Pa)	Silicone type	$\dot{\gamma}_d$ (s^{-1})	Prevailing style	Figure reference
Type 1 & 1a									
Decol.1[a]	1.2	0.4	1.5	175	52	PDMS	10^{-3}	HV	Figs. 4a, 5c
Decol.3[a]	1.2	0.7	1.5	175	9	MSR29	6×10^{-4}	HV	Fig. 4b
Decol.4	1.2	0.7	1.5	175	9	MSR29	6×10^{-4}	F-HV	Fig. 4d
Decol.5	1.6	–	1.5	199	–	–	–	FV	Fig. 5a
Decol.8	0.6	0.2	1.5	128	104	PDMS	2×10^{-3}	SDF	
Decol.6	1.2	0.2	1.5	175	104	PDMS	2×10^{-3}	FV	
Decol.9	1.8	0.2	1.5	223	104	PDMS	2×10^{-3}	CFHV	
Decol.2	1.2	0.4	1.5	175	52	PDMS	10^{-3}	F-HV	Figs. 4c, 5b
Decol.7	0.6	0.4	0.6	128	21	PDMS	4×10^{-4}	FV	Figs. 2a, 7d
Decol.13	1.2	0.4	0.6	175	21	PDMS	4×10^{-4}	F-HV	Fig. 2b
Decol.10	1.8	0.4	0.6	223	21	PDMS	4×10^{-4}	CFHV	Fig. 2c
Decol.14	0.6	0.4	0.6	128	0.3	MSR29 + OA	4×10^{-4}	HV	Fig. 2d
Decol.12	1.2	0.4	0.6	175	0.3	MSR29 + OA	4×10^{-4}	F-HV	Fig. 2e
Decol.11	1.8	0.4	0.6	223	0.3	MSR29 + OA	4×10^{-4}	FV	Fig. 2f
Decol.16[b]	1.2	0.4	1.5	175	52	PDMS	10^{-3}	F-HV	Fig. 6d
Decol.18[b]	1.2	0.4	0.6	175	21	PDMS	4×10^{-4}	F-HV	Fig. 6a, b
Type 2									
Det.Fd.36	0.2	0.4	0.6	96	21	PDMS	4×10^{-4}		Fig. 7c
Det.Fd.43	0.2	0.4	0.3	96	10	PDMS	2.1×10^{-4}		Fig. 3
Det.Fd.50	1	0.4	0.3	160	10	PDMS	2.1×10^{-4}		Fig. 3
Type 3									
Duct-L.Off.2	0.8/1.2	0.4	0.6	143/175	21	PDMS	4×10^{-4}		
Duct-L.Off.3	0.8/1.2	0.4	1.5	143/175	52	PDMS	10^{-3}		
Duct-L.Off.5	0.4/0.8	0.4	0.6	112/143	21	PDMS	4×10^{-4}		
Duct-L.Off.6	0.2/0.6	0.4	0.6	96/128	21	PDMS	4×10^{-4}		Fig. 7a, b

The Newtonian behaviour is expressed by the linear relationship between stress and strain rate $\tau_d = \eta\dot{\gamma}_d = \eta(v/H_d)$ where τ_d is the shear stress acting on the viscous layer, η the dynamic viscosity, and $\dot{\gamma}_d$ the engineering shear strain rate given by the ratio between the velocity v applied to the upper plate and the thickness of the viscous layer H_d. The engineering shear strain rate is generally used as an approximation for evaluating the strain rate in models where deformation in viscous layers is near simple shear ($\dot{\gamma}_d \approx \dot{\varepsilon}_m$) (e.g., Brun, 1999). The strain rate has been calculated at the onset of shortening, approximating v to the velocity of horizontal compression and taking H_d as the initial viscous layer thickness. Prevailing deformation style in Type 1 models: FV, foreland-verging thrusts; HV, hinterland-verging thrusts; F-HV, forethrusts followed by hinterland thrusts; CFHV, coeval fore and backthrusts; SDF, symmetric detachment folds. The exemplificative Type 2 models are from Bonini (2001).

[a] Initial model set-up with lubrication along the whole base of the silicone.

[b] Initial model set-up including a 3-cm-long lubrication in front of the moving wall.

e Georisorse, hosted by the Earth Science Department of Firenze. Models were properly scaled to nature and designed to simulate the vertical rheological stratification of a sedimentary cover with a ductile layer placed either at the base (Type 1) or embedded within (Type 2) a brittle overburden simulated by frictional material (dry sand). In Type 1a models, the silicone/Plexiglas floor box interface was lubricated with a thin layer of liquid soap to simulate a strong basal decoupling. In Type 3 models incorporating a lateral strength/rheological variation the silicone was offset. Depending on the model, the ductile décollement layer(s) was simulated by SGM 36 (PDMS), Mastic Silicone Rebondissant 29 silicone putties, or a mixture between Mastic Silicone Rebondissant 29 and oleic acid. Details of experiments (dimension, rheology and rate of deformation) are reported in Table 1 and below in Section 2.3.

Models were built in a Plexiglas squeeze box with internal dimensions 24 cm × 10 cm × 10 cm. Models had a length of 18–20 cm, width 10 cm, and total thickness varying from 0.8 to 2.2 cm depending on the experiment (Table 1). A thin plastic sheet placed at the sides of the squeeze box was lubricated with Vaseline oil in order to minimize sidewall boundary friction. Dry sand was sieved in the model with a 0.245 mm mesh. To visualize the internal deformation, the brittle part of the models consisted of layers of coloured sand used as passive markers. Models were shortened by driving a rigid vertical wall controlled by an electric motor at convergence rates varying between 0.6 and 1.5 cm h^{-1}. Models were shortened from 18% to 25% bulk shortening (BS) depending on the series of models.

In order to monitor the development and evolution of structures during deformation, lateral and top view photographs of the models were taken at regular time intervals. After deformation, the models were covered by dry sand to protect the final surface topography during water impregnation. Models were then frozen to allow cutting of undisturbed model cross-sections.

2.3. Model scaling and material properties

The physical models should necessarily represent a realistic replica of the natural prototype in terms or dimensions, rheology, and boundary conditions. Scaling of the models thus follows the principles of dynamic similitude reported in previous

pioneer works (Hubbert, 1937; Ramberg, 1981; Weijermars and Schmeling, 1986). Models are conveniently scaled such that 1 cm in the model represents 3 km in nature, thereby a length ratio $l^* = l_m/l_n = 3.3 \times 10^{-6}$ (Table 2). This implies that models simulate brittle overburdens ranging from 1.8 to 5.4 km in thickness, and 0.6–2 km-thick décollement layers (see Table 1). The adimensional factor of stress is therefore $\sigma^* = \sigma_m/\sigma_n = \rho^* g^* l^* = 1.9 \times 10^{-6}$, given $g^* = 1$ and $\rho^* = 0.56$ (Table 2).

The behaviour of the rocks composing the brittle overburden was simulated by dry quartz–feldspar sand obeying the Mohr–Coulomb criterion of failure (e.g., Davy and Cobbold, 1991). Laboratory tests on this material indicate a mean density $\rho_b \approx 1350$ kg m^{-3}, an angle of internal friction $\phi \approx 31°$, a coefficient of internal friction $\mu \approx 0.6$, and a cohesion $c \approx 80$ Pa. The behaviour of the rocks composing the viscous décollement layer has been simulated by transparent SGM 36 (PDMS) silicone (Weijermars, 1986) manufactured by Dow Corning Ltd., and pink Mastic Silicone Rebondissant 29 (MSR29, provided by CRC Industries, France). SGM 36 has a density $\rho_d = 965$ kg m^{-3}, and exhibits a Newtonian behaviour and dynamic shear viscosity $\eta = 5 \times 10^4$ Pa s at strain rates lower than 3×10^{-3} s^{-1} (Weijermars, 1986; Weijermars et al., 1993). Laboratory tests on the Mastic Silicone Rebondissant 29 indicate a density $\rho_d = 1120$ kg m^{-3}, and a Newtonian behaviour with dynamic shear viscosity $\eta = 1.5 \times 10^4$ Pa s (performed by a coni-cylindrical viscometer). The mixture of MSR29 with oleic acid resulted in Newtonian material with viscosity $\eta \approx 7 \times 10^2$ Pa s and density $\rho_d = 1060$ kg m^{-3} (Bonini, 2003).

Scaling down of model velocities to natural conditions yield values of the order of natural rates (Table 2). The dynamic scaling is taken as that discussed in Bonini (2003), where models were built with the same materials, deformed at similar rates, and had the same length and stress ratios. Model décollements composed of PDMS and MSR29-acid oleic mixture have been used to simulate strong and weak décollements reproducing natural salt viscosities of the order of 10^{19}–10^{20} Pa s and 10^{17}–10^{18} Pa s, respectively (Bonini, 2003).

3. Model results

Types 1 and 2 models exhibit typical, but different, deformation styles dictated by the initial set-up. In Type 1 models, the deformation can be schematically referred to a "floor-imbricate fan", where the thrust sheets are bounded by a floor thrust (or basal shear zone) localised in the lowermost part of the viscous décollement layer. Depending upon the boundary conditions, either thrust sheet arrays showing a dominant vergence or oppositely-verging thrusts may develop. In Type 2 models, the deformation is transferred to the ductile layer mostly by the imbricate foreland-verging thrusts developing in the floor sequence.

3.1. Brittle–ductile strength and deformation styles in Types 1 and 2 models

The transition between outward fold propagation (OFP) and typical passive-roof duplex (PRD) styles observed in Type 2 models has been related to the ratio and product of shear stresses at the base of the roof sequence (τ_b) and within the ductile layer (τ_d) (see Bonini, 2001, 2003). Those modelling results also suggested that the transition from OFP to the PRD field is mostly dependent upon an increase in the roof sequence strength τ_b.

Whereas Type 2 models show two clear structural domains, Type 1 models depict more complex deformation patterns that appear to be largely dependent upon the décollement strength τ_d. This behaviour is exemplified by the comparison between two sets of three Type 1 models. Both model sets had the same initial roof sequence thickness ($H_b = 0.6$ cm, $H_b = 1.2$ cm and $H_b = 1.8$ cm) and décollement thickness ($H_d = 0.4$ cm). However, the décollement of set 1 models was much stronger

Table 2
Scaling parameters

Parameter	Model (Decol.2 and 12; Type 1)	Nature	Model/nature ratio(*)
Density ρ_b, kg m^{-3}	1350	2400[a]	0.56
Density ρ_d, kg m^{-3}	965–1060	2200[a]	0.44–0.48
Viscosity η, Pa s	Decol.2; 5×10^4	$10^{19\text{ to }(20)}$[a]	$5 \times 10^{-15\text{ to }(-16)}$
	Decol.12; 7×10^2	$10^{17\text{ to }(18)}$[a]	$7 \times 10^{-15\text{ to }(-16)}$
Length l, m	0.01	3000	3.3×10^{-6}
Gravity g, m s^{-2}	9.81	9.81	1
Stress σ, Pa	159	2.9×10^6	$\sigma^* = \rho^* g^* l^* = 1.9 \times 10^{-6}$
Strain rate ε, s^{-1}	Decol.2; 10^{-3}	$2.6 \times 10^{-12\text{ to }(-13)}$	$\varepsilon^* = \sigma^*/\eta^* = 3.8 \times 10^{8\text{ to }(9)}$
	Decol.12; 4×10^{-4}	$1.5 \times 10^{-12\text{ to }(-13)}$	$2.7 \times 10^{8\text{ to }(9)}$
Time t, s	Decol.2; 3600	($t_n = t_m \sigma^*/\eta^*$) $1.4 \times 10^{12\text{ to }(13)}$ (0.045–0.45 Ma)	$t^* = (\varepsilon^*)^{-1} = 2.6 \times 10^{-9\text{ to }(-10)}$
	Decol.12; 3600	$9.7 \times 10^{11\text{ to }(12)}$ (0.03–0.30 Ma)	$4 \times 10^{-9\text{ to }(-10)}$
Rate of displacement v, m s^{-1}	Decol.2; 4.2×10^{-6}	($v_n = v_m \eta^*/\sigma^*\ l^*$) $3.3 \times 10^{-9\text{ to }(-10)}$ (100–10 mm yr^{-1})	$v^* = l^*/t^* = 1269$–12692
	Decol.12; 1.6×10^{-6}	$2 \times 10^{-9\text{ to }(-10)}$ (56.6–5.6 mm yr^{-1})	891–8910

The model to nature dimensionless ratios are indicated with the asterisk. Subscripts m and n refer to model and nature, while subscripts b and d refer to brittle and ductile layers, respectively.

[a] Parameters indicating average values.

($\tau_d = 21$ Pa) than that of set 2 models ($\tau_d = 0.3$ Pa) (Fig. 2 and Table 1).

With increasing H_b and τ_b, in set 1 models there is a transition from foreland-verging thrusting (model Decol.7; $H_b = 0.6$ cm) to dually-verging thrusts consisting of either backthrusts superimposed onto former forethrusts (model Decol.13; $H_b = 1.2$ cm), or coeval forethrusts and backthrusts (model Decol.10; $H_b = 1.8$ cm) (Fig. 2a–c). By contrast, in set 2 models the deformation style varies from dominant backthrusts (model Decol.14; $H_b = 0.6$ cm), to dually-verging thrusts (model Decol.12; $H_b = 1.2$ cm), to a long-lasting single forethrust (model Decol.11; $H_b = 1.8$ cm) (Fig. 2d–f). This behaviour shows clearly the sharp variations in thrust wedge deformation in relation to the brittle–ductile coupling, as well as to the magnitude of décollement strength τ_d.

In the attempt to compare the results of the different model types, the deformation styles observed in Type 1 models have been plotted on the diagram stress ratio (τ_b/τ_d) versus stress product ($\tau_b\tau_d$) used for Type 2 models (Fig. 3). In this diagram, the set 1 model data points fall in the lower part of the OFP–PRD transition curve, in the sector with relatively low stress ratio and high stress product. Set 2 models fall instead in the upper part of the same curve with high stress ratio and low stress product (Fig. 3). This analysis gives further emphasis to the dissimilar behaviour of sets 1 and 2, which can be taken as representative of "normal" and "weak" décollements, respectively. As a matter of fact, the deformation trends appear to be somehow opposite, as forethrusting develops in set 1 when H_b is minimum, and in set 2 when H_b is maximum (Figs. 2 and 3).

The PRD–OFP transition deduced for Type 2 model seems to involve some meaning for Type 1 models also. A large variety of deformation styles fall indeed on this boundary, such as backthrusts (model Decol.14), forethrusts (model Decol.7), and symmetric box folds (model Decol.8) (Fig. 3). Dually-verging thrust faults fall instead in the (Type 2) PRD field. Ultimately, it is worth noting the presence of an alignment of model data points broadly connecting the middle part of the constant-τ_d curves (Fig. 3). These data points correspond to dually-verging thrusts in which backthrusts are clearly superimposed onto forethrusts (white squares in Fig. 3). Thicker

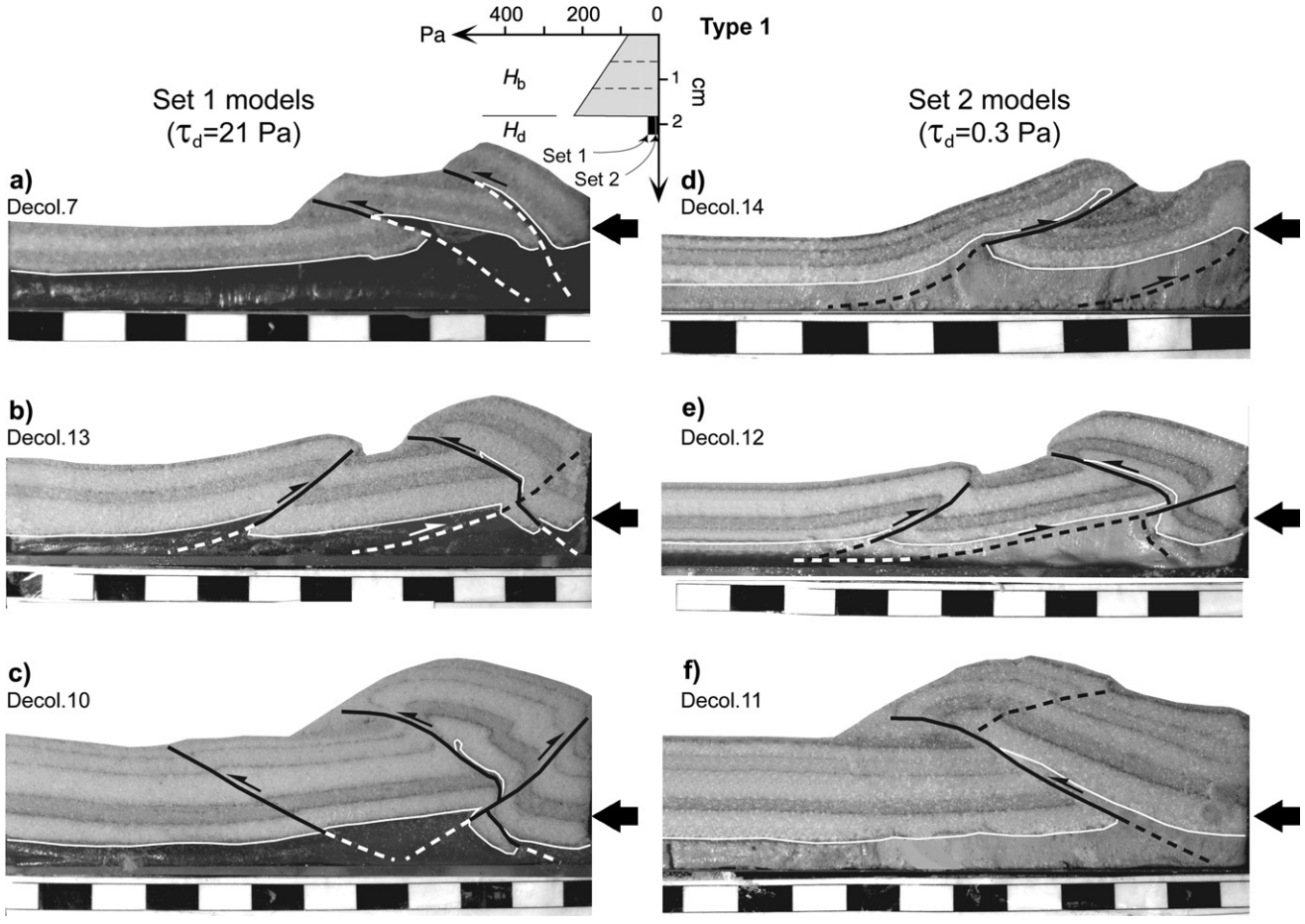

Fig. 2. Deformation styles in Type 1 models as a function of the roof sequence and décollement strengths (τ_b and τ_d, respectively). This behaviour is represented by the shear strength profile on top of the figure, and is illustrated by the comparison between two sets of models performed with "normal" and "weak" décollement strength ($\tau_d = 21$ Pa and $\tau_d = 0.3$ Pa, respectively). For comparison, the models were deformed at the same bulk shortening (18% BS). H_d is the thickness of the ductile silicone layer, H_b is thickness of the brittle roof sequence. The thin white lines indicate the top of the silicone layer. Thick black arrows indicate the direction of the moving wall. The ruler at the base of all models is in centimetres. See text for details.

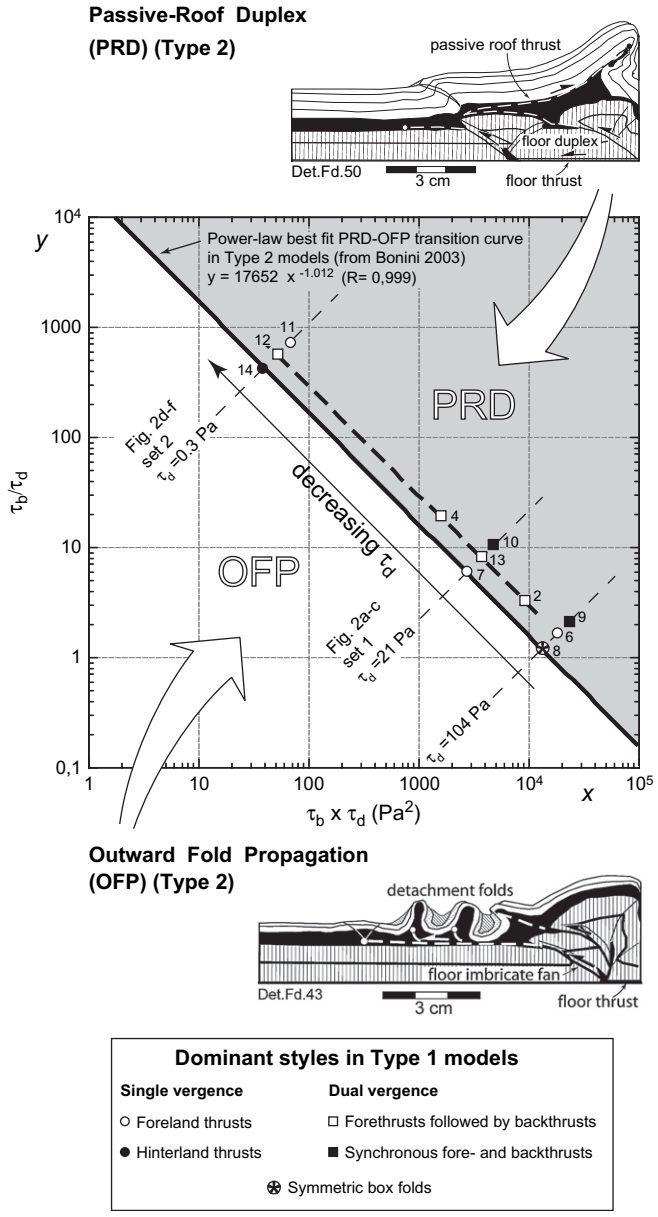

Fig. 3. Model deformation styles as a function of shear stress at the base of the roof sequence (τ_b) and within the décollement (τ_d). Type 1 data points have been plotted onto the diagram stress ratio (τ_b/τ_d) against stress product ($\tau_b\tau_d$) showing the separation between passive-roof duplex and outward fold propagation domains (outlined by typical OFP and PRD style models) in Type 2 models (from Bonini, 2003). Numbers beside the ornaments (circles, squares) indicate the Type 1 experiment's number in Table 1. Note that a similar diagram could be constructed for natural conditions converting the model shear stresses by the adimensional factor of stress σ^* (e.g., Bonini, 2001, 2003).

overburdens promote instead the development of coeval (and competing) forethrusts and backthrusts (black squares in Fig. 3), thus suggesting a near horizontal stress σ_1 axis. The above analysis may also indicate that the structural patterns developing in Type 1 models are apparently more sensitive to the absolute shear stress values than Type 2 models, which were characterised by a clear OFP–PRD transition for a wide range of shear stress ratios and products.

3.2. Basal friction and deformation patterns on single décollement (Type 1a models)

Type 1a models (Section 2.1.2) effectively exemplify the effect on brittle overburden deformation produced by a strong decoupling horizon at the base of the décollement layer. The comparison between models built with (Type 1a) or without (Type 1) such a decoupling horizon is straightforward (see Fig. 4). Whereas the presence of the basal decoupling favours the development of a thrust sheet array with predominant hinterland vergence (models Decol.1 and 3; Fig. 4a, b), models not incorporating such a feature show a less defined structural vergence, as either foreland-verging thrusts and symmetric box folds (model Decol.2), or doubly-verging thrusts (model Decol.4) may develop (Fig. 4c, d; Table 1).

In agreement with previous authors (Dickinson and Seely, 1979; Byrne et al., 1993), the results of modelling suggest that very low basal friction may represent a key parameter able to determine the development of a preferred hinterland thrust vergence. Foreland vergence will instead dominate when basal friction increases. In this regard, the orientation of the maximum compressive σ_1 axis is crucial because of its relation to deformation. The development of contrasting deformation styles can be thus related to the angle ψ_b, the dip of the σ_1 axis with respect to the basal décollement (e.g., Davis and Engelder, 1985). Since failure planes are symmetrical (i.e., same θ) with respect to the principal σ_1 axis (Hafner, 1951), the orientation of this axis can be estimated by measuring the dip of the conjugate thrust faults in the models (Davis et al., 1983; Dahlen et al., 1984; see Fig. 5a–c).

Since the décollement layer is horizontal, the fault dip equals the step-up angle δ (Figs. 1a and 5a–c). The angle θ between the σ_1 axis and the fault plane is expressed by Anderson (1951) as $\theta = \pm 45° - 1/2 \tan^{-1}\mu$, thus the magnitude and the orientation of the angle ψ_b can be readily estimated knowing that, for $\mu \approx 0.6$ as in our material, $\theta \approx 29.5°$. The angle ψ_b is thus determined by $\psi_b = \theta - \delta_f$ in case of forethrust step-up angles, and by $\psi_b = \delta_b - \theta$ for backthrust step-up angles (Davis and Engelder, 1985; Figs. 1a and 5a). The angle ψ_b may be either positive (σ_1 dipping toward the foreland) or negative (σ_1 dipping toward the hinterland) in respect to the basal thrust detachment (see Fig. 1a). Accordingly, the dip of newly formed faults measured in the models suggests an obvious positive inclination of the stress σ_1 axis in purely frictional models ($\psi_b \approx 5°$ in model Decol.5; Fig. 5a), a significant but negative inclination of the σ_1 for Type 1a models ($\psi_b \approx -3°$ to $-5°$ in model Decol.1; Fig. 5c), and a near horizontal orientation ($\psi_b \approx 1°$) of the same axis for Type 1 models (model Decol.2; Fig. 5b).

The different orientation of the σ_1 axis in Type 1 and 1a models may be associated with the development of dissimilar velocity profiles within the basal décollement layer depending upon basal friction (Fig. 5b, c). Despite the sense of absolute basal shear being the same in all models, a different strain partitioning has likely resulted from the relative velocity between the upper and lower silicone boundaries, thereby resulting in a different sense of relative shear within the ductile layer

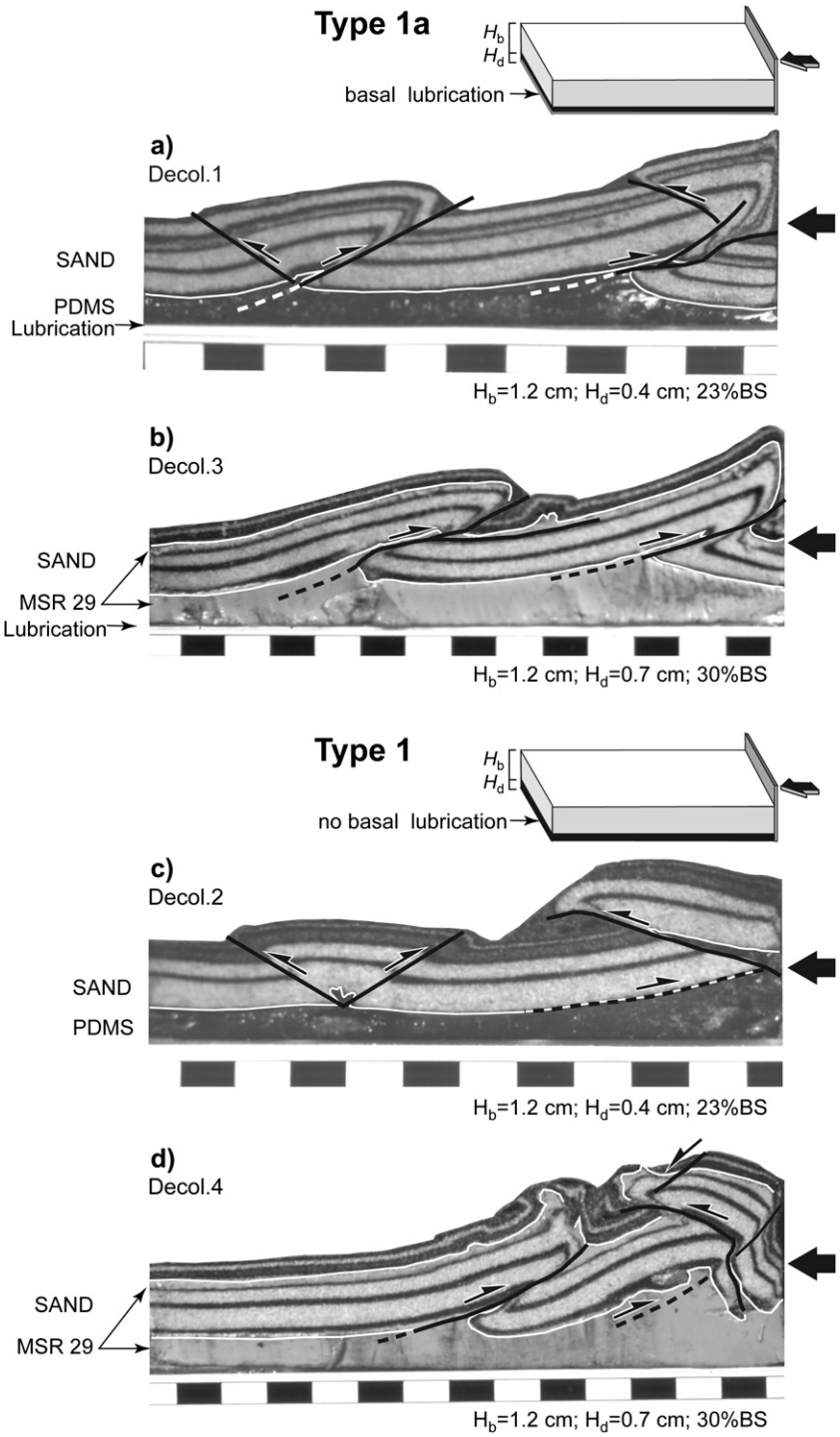

Fig. 4. Comparison between model cross-sections of Type 1 and 1a models. The presence of basal lubrication (Type 1a) invariably resulted in predominant hinterland-verging structures. The absence of such a basal lubrication (Type 1) resulted instead in dually-verging thrusts and/or box folding. In (d), the backthrust close to the backstop developed as late deformation superposed onto a forethrust. Models were deformed under the same shortening rate (1.5 cm h^{-1}) but at different bulk shortening. Note the foreland-tapering silicone wedge at the base of models.

(Fig. 5b, c). In this hypothesis, the basal coupling controls the sense of ductile shear, and ultimately the orientation of the σ_1 that will rotate consistent with the sense of bulk décollement shear (Fig. 5a–c). Thus, in Type 1 models the σ_1 axis will slightly rotate in the same direction as the applied shortening (foreshearing). Conversely, in Type 1a models the σ_1 axis will rotate oppositely to the applied direction of shortening (backshearing). Consequently, the backthrusts will dip more gently than forethrusts, and will be thus favoured (Fig. 5c).

The different mechanical behaviours described above can be synthetically illustrated by a Mohr–Coulomb diagram. The shear stress is considered positive or negative when produces a counterclockwise or clockwise rotation (torque) of a body (in our case foreshear or backshear within the basal

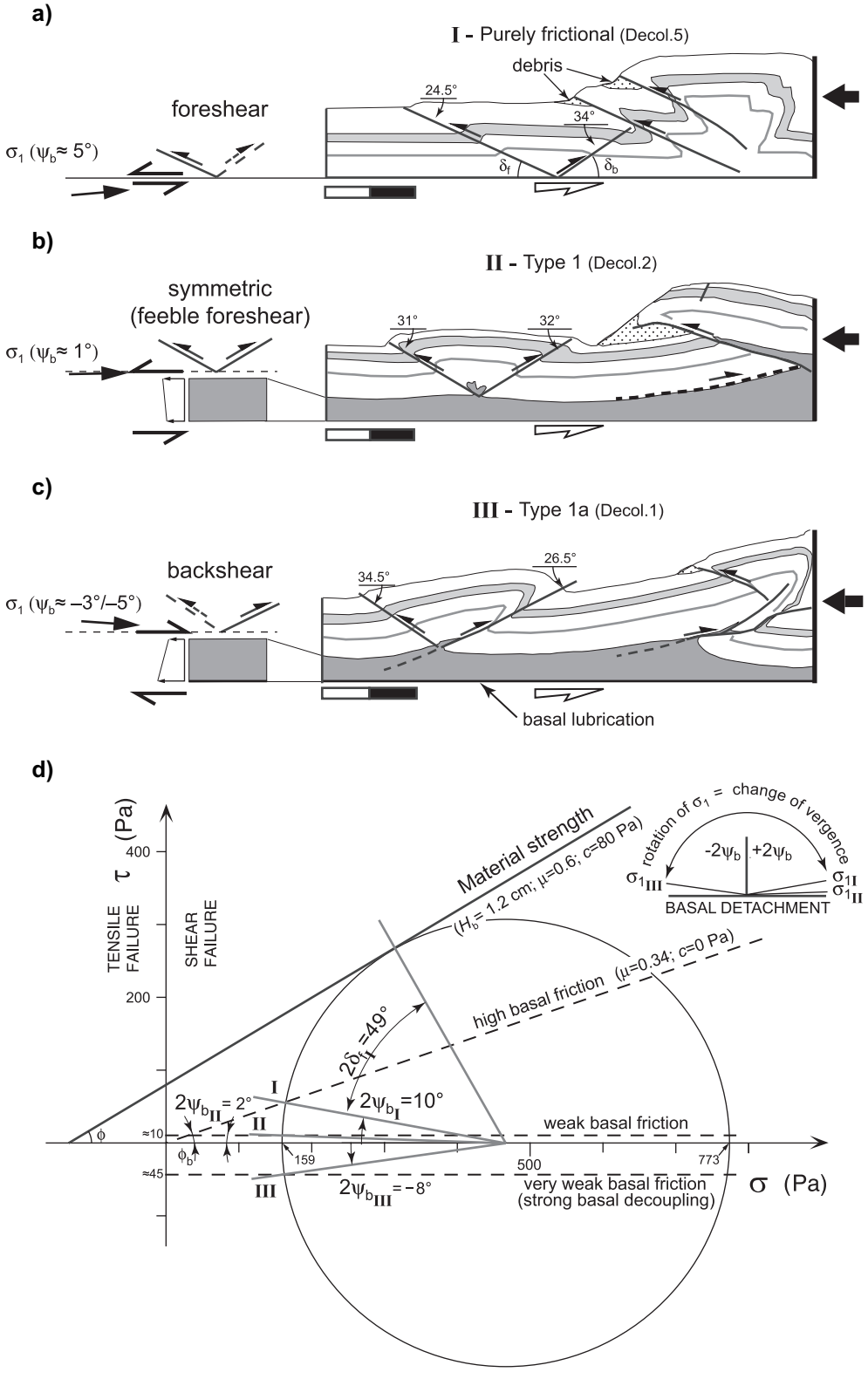

Fig. 5. Estimation of the σ_1 axis orientation in (a) purely frictional, (b) Type 1, and (c) Type 1a models, by matching fault dip and angle θ ($\approx$29.5°). The hypothetical velocity profiles configuring in the ductile décollement layer in relation to basal friction are schematically reported in (b) and (c), together with the inferred sense of shear. The white arrow indicates the sense of basal shear. The Mohr circle in (d) has been adapted to models Decol.1–5 (where $H_b = 1.2$ cm, $\rho_b = 1350$ kg m^{-3}, $\mu = 0.6$, c = 80 Pa). I, II, III refer to the angle ψ_b (between the σ_1 axis and the basal detachment) in models Decol.5, 2 and 1, respectively. Dashed lines indicate (frictional or viscous) sliding on décollement. The angle $\psi_b \approx 5°$ obtained form the purely frictional model suggests a drop of $\approx$40% of the friction coefficient at the Plexiglas/sand interface.

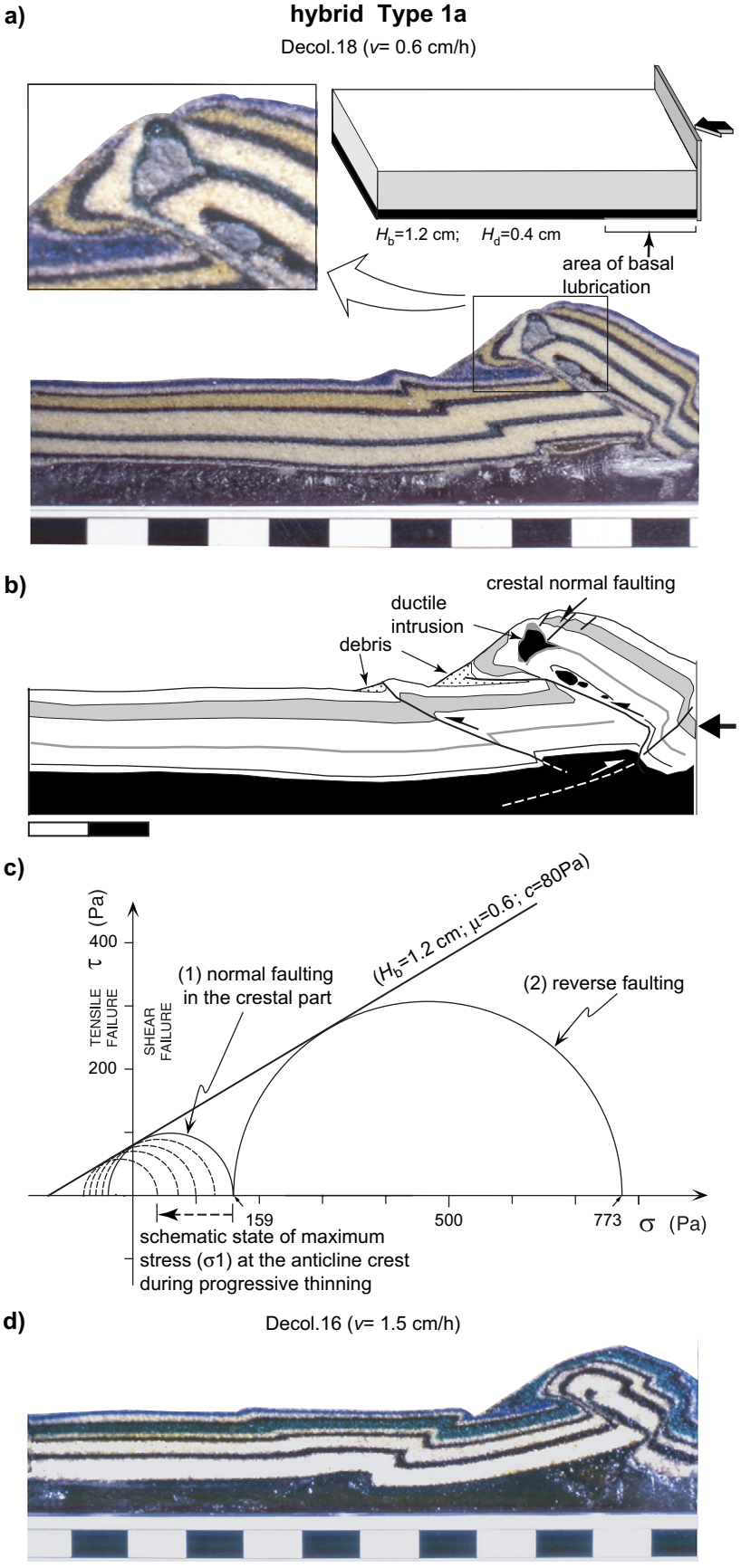

Fig. 6. (a) Diapiric ductile intrusion at the brittle core of an experimental thrust-related fold that evolved from early detachment fold to late breakthrough thrust (model Decol.18). (b) Interpretative line-drawing highlighting the major features. (c) Mohr circle illustrating the different states of stress in the model, with

décollement), respectively (Fig. 5d). In the Mohr diagram, the measured angles ψ_b suggest that the basal shear stress in Type 1a models should be significantly higher than in Type 1 (cf. $\psi_{b_{II}}$ with $\psi_{b_{III}}$ in Fig. 5d). This behaviour is likely related to a strain localization process promoted by the basal lubrication, and could explain the significant back rotation of the σ_1 axis inferred for Type 1a models.

3.3. Implications for diapirism at detachment folds (hybrid Type 1a models)

In some experiments the liquid soap at the base of the silicone was restricted to a 3 cm-long strip in front of the moving wall (hybrid Type 1a models; see model set-up in Fig. 6). These models invariably resulted in the development of an early-single-detachment fold localised by the basal thrust tip controlled by the external soap boundary (Fig. 6a). The folds were successively squeezed laterally, overturned, and a forethrust pinched the ductile core and faulted the forelimb. A late backthrust displaced the previous structures (Fig. 6a, b). Notably, some detachment folds exhibited intrusions of ductile material within the crestal area. Such ductile masses show discordant contacts with the brittle overburden, and can be therefore reasonably referred to diapiric-like structures (Fig. 6a, b). The development of this structural pattern was, however, very sensitive to model construction, as diapiric patterns were observed in two of the three control models performed to test reproducibility.

The above structures are basically similar to the examples of viscous material pinched-off in the core of the experimental anticlines reported in Koyi (1998), though no diapirs could penetrate the overburden units of those models. Despite the different boundary conditions, the current results look also similar to the development of diapirs breaking the crest of the most internal thrust anticline observed in models by Costa and Vendeville (2001). Likewise the present modelling, the development of such a diapirism was controlled by a rheological contrast built in the basal décollement (hinterland pinch-out).

A possible mechanism explaining the penetration of the brittle overburden can be related to the marked strain localization (at the basal thrust tip) promoting relevant fold amplification. The ductile material can be thus transported at shallower levels in the core of thrust-related folds. With increasing shortening and fold amplification, normal faults stretch the hinge and crest of the detachment fold. The presence of these structures suggests a (transient) near vertical σ_1 axis, which implies a minor shear strength in comparison to that of a compressional regime (Fig. 6c). This effect is enhanced by the slumping from the model anticline crest. Both normal faulting and slumping would result in a positive feedback reducing progressively the shear strength in the crestal area (Fig. 6c). Upward flow of ductile material and thinning of the anticline crest are therefore expected to have produced the observed deformation outcome (Fig. 6). Preliminary models deformed with higher strain rates did not develop diapirism (e.g., model Decol.16; compare Fig. 6a with d). This behaviour suggests that the lower strain rate favoured a comparatively higher amplification of the early detachment fold, which achieved the potential for developing diapirism.

3.4. The role of transverse faults (Type 3 models)

Brittle–ductile analogue models applied to the Salt Range in Pakistan (Cotton and Koyi, 2000) suggest that lateral rheological contrast may also provide a key for understanding the occurrence of dominating hinterland-verging thrusts. Transverse (transfer or strike-slip) faults may juxtapose sediments with different rheological properties, a pattern that is expected to produce a change in structural style across the fault(s). This factor has been investigated by some test models in which the silicone layer was offset by a vertical fault plane parallel to the longer side of the box. Half of the model had the silicone layer in contact with the Plexiglas floor box, while the silicone was embedded in the sand pack in the other half part. The models were shortened parallel to this rheological boundary, and the thickness of the upper brittle layer and the rate of shortening were varied depending on the model (Table 1).

Preliminary results show that this model configuration often resulted in the development of dominating backward verging thrusts in both model halves. Such a deformation pattern is exemplified by model Duct-L.Off.6 (Fig. 7a, b). Dominant backthrusts developed in the model half with silicone at the base, whereas in the correspondent Type 1 configuration the direction of thrusting was opposite (cf. Fig. 7b with d). Likewise, the other model half (with the embedded silicone) shows dominant backthrust folds, which are not observed in the correspondent Type 2 model where thrust folds were mostly symmetrical (cf. Fig. 7a with c).

The above observations may suggest that the presence of a lateral rheological/strength variation is able to influence the orientation of σ_1. As a corollary, one may argue that this boundary may produce a stress field perturbation rotating the σ_1 axis opposite to what happens in models deformed without such a built-in rheological change.

4. Discussion: modelling results and comparison with nature

The present modelling aimed not to simulate specific natural cases, rather to obtain some clues about the factors controlling some general features that characterise many natural fold-and-thrust belts. Though models represent a simplified replica of the natural prototype, the mechanical consistency of

a comparatively less resistant crestal part. This latter condition is inferred from the development of normal faulting over the anticline crest that should have facilitated the penetration of the ductile diapir. Dashed Mohr circles schematically represent differential stress decrements in the fold crest owing to the thinning produced by normal faulting and slumping. (d) Cross-section of model Decol.16 deformed with a higher rate of shortening (keeping the initial set-up as in model Decol.18). In this case, diapirism did not develop.

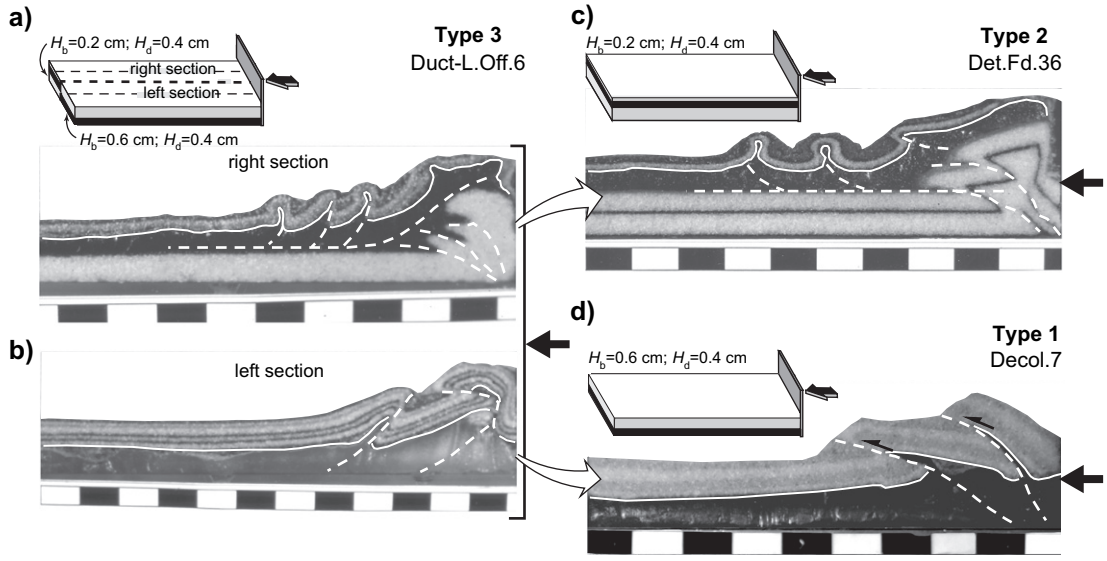

Fig. 7. Comparison of Type 3 model Duct-L.Off.6, incorporating a vertical longitudinal rheological boundary, with the corresponding Types 1 and 2 models not including such a feature. Models were deformed under the same shortening rate (0.6 cm h^{-1}) and bulk shortening (18% BS). See text for details.

scaled models can offer a realistic picture of basic deformation geometries. The experimental results suggest an intimate link among deformation style, shear stresses and initial model set-up. These results are discussed separately below, by also reference to the natural archetypes reported in Fig. 1.

4.1. Foreland and hinterland-verging thrust faults on single décollement

The observation that fold-and-thrust belts generally exhibit a foreland vergence is apparently at odds with the fact that they are commonly detached above a décollement, which should instead favour dually-verging belts (Fig. 1d). Previous experimental work approached this problem and concluded that the preferential development of forethrusts (detaching on a single décollement) is favoured by the presence of décollement pinch-outs (Costa and Vendeville, 2002), and by strong brittle–ductile coupling (Smit et al., 2003).

The current Type 1 models highlight the importance of shear stresses τ_b and τ_d in controlling the preferential development of forethrusts. In nature, shear stresses depend upon the geometry of the brittle and ductile layers, pore fluid pressure, strain rate and viscosity. In case of a relatively strong décollement, dominant forethrusts developed for relatively low brittle–ductile shear stress ratios, that is high brittle–ductile coupling (models Decol.6 and 7; Fig. 3). Conversely, with a weak décollement dominant forethrusts developed for relatively high shear stress ratios thereby low brittle–ductile coupling (model Decol.11; Fig. 3). This behaviour may suggest that the development of forethrusts might be not simply depending on the magnitude of the brittle–ductile coupling, but it could also depend upon the absolute value of décollement strength in relation to brittle overburden strength. Such absolute values may be compared to nature by converting the model shear stresses by the adimensional factor σ^*, which is given as $\sigma^* = \sigma_m/\sigma_n = 1.9 \times 10^{-6}$. As a corollary, the strain rate (likewise décollement pinch-outs) may represent an important independent variable controlling the deformation style, as even high-viscosity décollements may attain feeble shear strength at very low rates.

Though the preferential development of hinterland (landward)-verging thrusts is uncommon elsewhere the Cascadian margin (Fig. 1e), various complementary models have been proposed to explain this peculiar behaviour: (1) feeble basal friction (Dickinson and Seely, 1979; McKay et al., 1992; Byrne et al., 1993), (2) a combination of very low basal shear stress and basal dip (MacKay, 1995), and (3) strain-rate control in non-Coulomb wedges (Gutscher et al., 2001). The results of the present modelling suggest that additional causes may promote the development of preferential backthrusts in Cascadian-type wedges, such as:

(1) back rotation of the σ_1 axis (Type 1a models; Figs. 4a, b and 5c), which may be favoured by the presence of an horizon of mechanical weakness at the base of (or within) the viscous décollement layer. In natural shale décollements, rheological weaknesses are expected to be localised by overpressured pore fluid conditions that are, in turn, controlled by spatial differences in material properties. For instance, the intrinsic mechanical weakness of smectite-rich horizons may influence the position of fault zones, and the tendency of smectite-group clays to generate pressure swells probably contributes to the generation and localization of excess pore pressures within the décollement (e.g., Vrolijk, 1990; Deng and Underwood, 2001). Likewise, salt at the base of (or embedded in) a manly anhydrite décollement may provide zones of very weak mechanical strength.
(2) specific shear stress conditions, which configured in Type 1 models only for relatively low shear stress product and

high shear stress ratio in case of weak model décollements (model Decol.14 of set 2; Figs. 2d and 3).

(3) across-strike rheological variations (Type 3 models; Fig. 7). This possibility is corroborated by the observation that transverse faults accommodating differential sedimentation and displacing potential décollement layers have been identified in the Cascadian margin (MacKay, 1995).

The above discussion suggests that several causes may potentially control the development of a preferred hinterland or foreland thrust polarity. These causes may operate independently or contribute together, so that it may be difficult to determine the operating factors, or dissect the net effect into all of the contributing causes. The difficultly in assessing the natural controlling factors may be exemplified by considering the estimation of the ductile shear stress, which has been shown to strongly influence the deformation outcome. Shear stress is essentially defined by strain rate and décollement viscosity, factors that are, however, often poorly known. The lack of knowledge of the past and/or present shear stresses may thus inhibit at a large extent the definition of the factors potentially controlling thrust polarity in natural prototypes.

Lastly, it is worth noting that the hybrid Type 1a models are potentially able to trigger diapirism at the core of a detachment fold, implying that ductile diapirs can potentially develop in settings dominated by shortening. Thus, it is not necessary that diapirism developed in thrust wedges should have been invariably triggered by an early extension phase preceding the compression (e.g., Jackson and Vendeville, 1994).

4.2. Thrust triangle zones on single décollement and inversion from foreland to hinterland thrust polarity, with examples from the Apennines

Model thrust triangle zones developing above a single décollement exhibited typical fore and backthrusts that formed either alternated or coeval during shortening. The analysis of Type 1 and 1a models has revealed a clear tendency to develop a sequence of thrusting consisting of early forethrusts deformed by late backthrusts (see Figs. 2b, e and 6). This behaviour occurs for model data points (white squares) falling in an intermediate region of the shear stress ratio/shear stress product diagram; this tendency is illustrated by the thick dashed line in Fig. 3.

The inversion from foreland to hinterland thrust polarity would suggest a late (back)rotation of the principal σ_1 axis, thereby a progression from foreshear to backshear within the décollement. This evolution is likely favoured by the configuration of a growing ductile wedge tapering toward the foreland (see Fig. 4a–d), and increasingly sloping with shortening. The upper part of this foreland-dipping silicone wedge thus represents a favourably-oriented rheological boundary along which back thrusting may take place.

The effect of buttressing provided by the distal fixed wall would be also essential in such a reversal of thrust polarity. Buttresses are common features in fold-and-thrust belts that may develop (1) prior of shortening, when the main décollement(s) is originally displaced by syndepositional growth faults juxtaposing weak and hard rocks, or (2) during shortening, for instance when the main décollement is displaced by multiple-phase out-of-sequence thrusting generating thrust-related basement highs, thereby multiple décollement pitchouts. Such effects are also possible when salt welds are formed during formation of pop-downs that limit the flow/migration of the viscous layer (e.g., Cotton and Koyi, 2000). In addition, the synshortening thickening of both the roof sequence (by folding and thrusting) and the ductile layer tend to decrease the brittle–ductile coupling (by increasing τ_b and decreasing τ_d, respectively). Smit et al. (2003) noted in fact that backthrusts invariably developed in the more decoupled parts of the wedges. The observation that this chronology of deformation has been mostly recognised in the internal part of the models may also accord with the hypothesis by Davis and Engelder (1987) that a thrust-related increase in topography could favour the back rotation of the σ_1 axis, thereby backthrusting.

Applying the lessons of modelling to natural cases, the Apennines fold-and-thrust belt is taken as an example in which the tendency of backthrusts to displace earlier foreland-verging structures can be documented both in the foreland and hinterland sectors. In the foreland of the Southern Apennines, Doglioni et al. (1999) identified two distinct and oppositely-verging sedimentary Miocene wedges – specifically an hinterland pinching-out wedge overlying a foreland pinching-out wedge (Fig. 8a, b). In addition, thrust faults emanated from the regional floor thrust show late backthrusts systematically displacing early forethrusts. This setting thus documents the inversion from foreland to hinterland-directed thrusting in the frontal foredeep of the Southern Apennines.

Similarly, forethrusts and backthrusts have controlled the evolution of the major Miocene–Pliocene Siena–Radicofani Basin in the Northern Apennines hinterland (Bonini and Sani, 2002). These dually-verging structures formed above the thick Burano Fm. which is a $\approx$1 km-thick layer of evaporitic rocks composing the main Northern Apennines décollement (Baldacci et al., 1967) later displaced by basement thrusting (Bally et al., 1986; Finetti et al., 2001). A chronology of deformation between these structures is suggested by seismic line interpretation, in which backthrusts are imaged to displace former E-verging thrust fold structures (Fig. 8c, d). In the seismic line, the backthrust is imaged to surface at the eastern margin of the Siena–Radicofani Basin, consistently with the presence of a WSW-verging overturned syncline in the Pliocene conglomerates (Fig. 8e).

4.3. Passive-roof duplex development

The parameters governing the development of passive-roof duplexes have been examined in detail by a number of recent numerical (Erickson, 1995; Jamison, 1996) and analogue modelling works (Mugnier et al., 1997; Bonini, 2001; Couzens-Schultz et al., 2003). Beside the necessary presence of suitable décollement layers within, or at the base of the sedimentary cover (e.g., Couzens and Wiltschko, 1996), the development

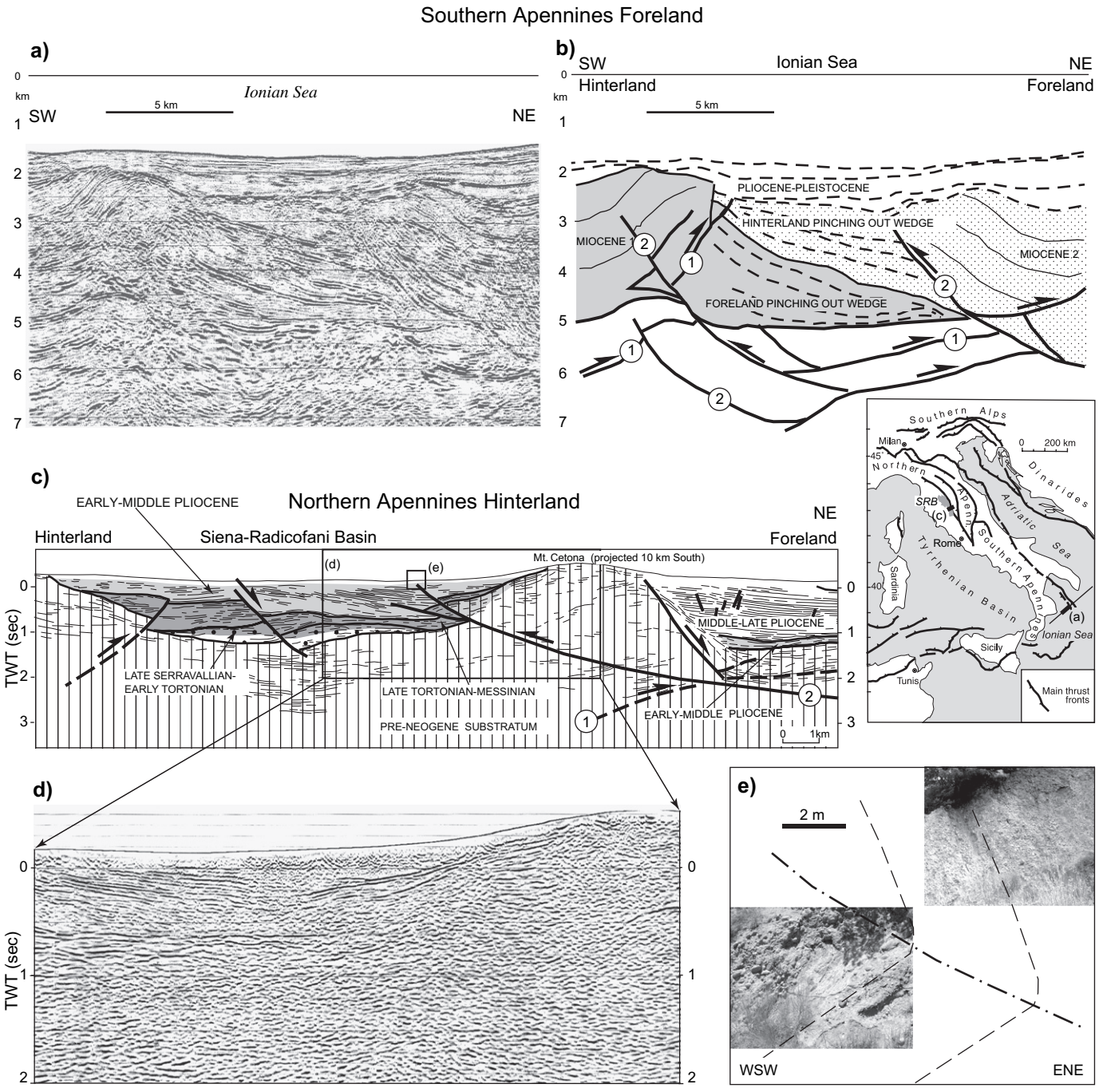

Fig. 8. Examples from the Apennines fold-and-thrust belt of foreland thrusts deformed by successive hinterland-directed thrusting. Encircled numbers 1 and 2 indicate the chronology of faulting. (a) Seismic line and (b) interpretative sketch of the Ionian foredeep in Southern Apennines (after Doglioni et al., 1999). (c) Interpretative line-drawing of a seismic section crossing the Siena–Radicofani Basin (SRB) in the Northern Apennines hinterland (modified after Bonini and Sani, 2002). (d) Detail of the seismic line showing a late backthrust displacing the bottom of the basin. (e) Reconstructed overturned syncline in Pliocene deposits at the surfacing of the backthrust (location in c).

of triangle zones may be promoted by a number of contributing factors, such as: (1) synshortening erosion unloading the roof thrust hangingwall (Mugnier et al., 1997), (2) frontal sedimentation providing a minimum critical thickness (i.e., strength) of the roof sequence (Bonini, 2001), (3) the effect of frontal buttressing and décollement strength (Erickson, 1995; Jamison, 1996; Couzens-Schultz et al., 2003; Koyi and Sans, 2006). In their detailed analysis, Couzens-Schultz et al. (2003) propose two passive-roof duplex end-members, (1) a prograding frontal monocline (Jones, 1996; Figs. 1f and 9a), and (2) spaced ramp anticlines locally underthrusting the cover (Fig. 1g).

In finite-element models incorporating a distal buttress and a weak roof décollement, the deformation results in relevant underthrusting and thus in thrust triangle zone development (Erickson, 1995; Jamison, 1996). In analogue models with weak roof décollement and without foreland buttressing, Couzens-Schultz et al. (2003) observed that deformation was instead dominated by forethrusting and active-roof duplexes in which the stress was transmitted forward thrust horse blocks (Fig. 9b). The presence of a strong roof décollement results in more similar deformation patterns either with or without buttressing. Décollement pinch-outs and strength contrasts can also effectively determine the development/style of thrust triangle zones (Koyi and Sans, 2006).

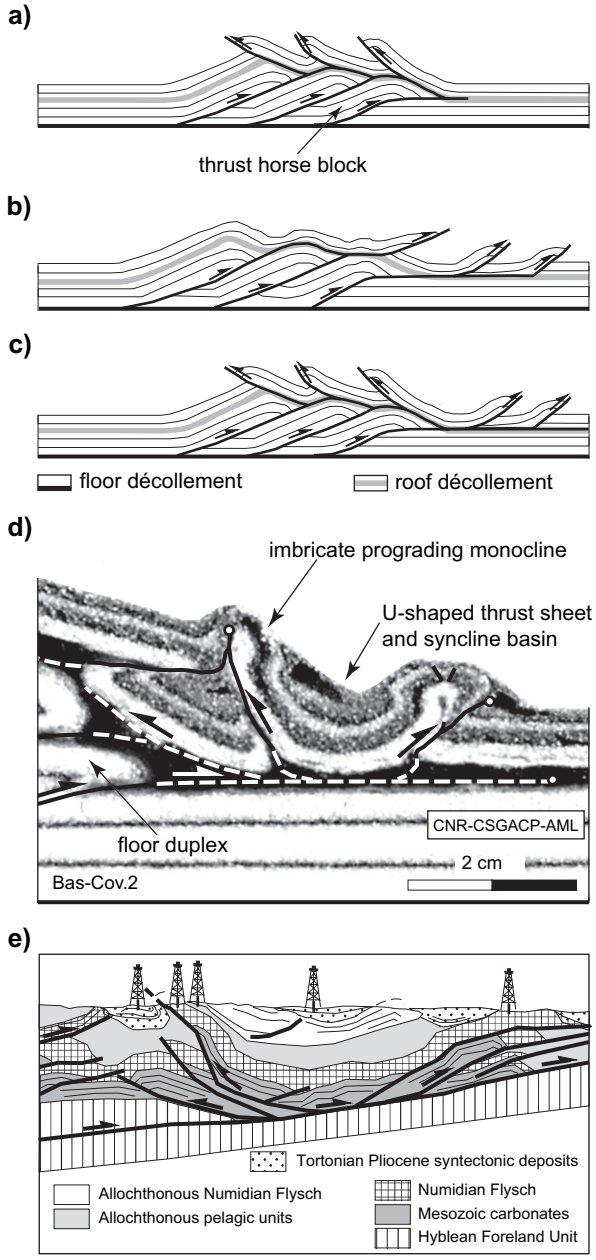

Fig. 9. (a) Passive- and (b) active-roof duplex (from Couzens-Schultz et al., 2003), and (c) ''composite-roof duplex'' model (present work), which is exemplified by (d) a cross-section photograph of Type 2 model Bas.Cov.2 (from Bonini and Sani, 2002). Note the U-shaped thrust sheet geometry creating a potential syncline basin in front of the floor duplex. This model structural pattern appears to be striking similar to the main deformation style at the front of the Apenninic-Maghrebian fold-and-thrust belt in Eastern Sicily (e; redrawn after Bello et al., 2000).

The models by Couzens-Schultz et al. (2003) showed deformation styles close to the passive-roof duplex mode with spaced ramp anticlines, whereas no underthrusting at a regional scale similar to a prograding frontal monocline mode was observed. These authors concluded that, following Mugnier et al. (1997), the factor likely controlling the development of a prograding frontal monocline is erosion, which removes the upper part of the growing monocline. However, the roof sequence thickness has been demonstrated to exert also some control on the deformation style at mountain fronts (see model Det.Fd.50 in Fig. 3). This is suggested by the observation that the progression from outward fold propagation (equivalent to the concept of active-roof duplex) to a prograding monocline style was mostly controlled by an increase in the roof sequence thickness irrespective of the décollement strength (Bonini, 2003). It is not surprising therefore that the typical prograding monocline described in Banks and Warburton's (1986) pioneer work was characterised by a very large thickness (about 8 km) of the syntectonic roof sequence at the Pakistan range front. On the other hand, the roof sequence thickness alone is not able to produce the typical setting of a single prograding frontal monocline, in which the roof sequence ahead the monocline is essentially undeformed (e.g., Alberta foothills, Price, 1981, and frontal Pakistan, Banks and Warburton, 1986; Fig. 1f). Imbricate prograding frontal monoclines have been also described in Couzens-Schultz et al. (2003).

The observation that some frontal areas of fold-and-thrust belts are characterised by the coeval development of a prograding frontal monocline and outward propagation of deformation (e.g., Amadeus Basin in Fig. 1h) may suggest the occurrence of a third deformation model in-between the active and passive-roof duplex end-members. Such an additional model is referred to here as ''composite-roof duplex'' (Fig. 9c). The composite-roof duplex is exemplified by the results of Type 2 model Bas-Cov.2 (Fig. 9d), which can be strikingly matched with the geometry of the Apenninic–Maghrebian chain front in Eastern Sicily (Bello et al., 2000; Fig. 9e). An imbricate prograding frontal monocline associated with active-roof thrusting can be indeed inferred in both cases. The model and the natural prototype show also a characteristic U-shaped thrust sheet geometry in front of the floor duplex, which is being generated, in the natural case, by the thrusting in the Hyblean Foreland Units (Fig. 9e).

The comparison with the models by Mugnier et al. (1997) suggests that the difference between true passive-roof duplexes and composite-roof duplexes could be the application of a minimum amount of erosion unloading the growing passive-roof thrust hangingwall. When erosion does not reach such a critical value, more shear stress is transmitted forward the frontal monocline, and consequently the roof sequence fails by folding and thrusting (see the Amadeus Basin in Fig. 1h).

The conclusions illustrated in the previous Section 4.2 (and applied to thrust triangle zones developing on a single décollement) can be also taken as valid for the outward deformation ahead of a thrust horse block indenting the roof décollement in composite-roof duplexes. This setting would be a rather common feature, as in many cases dually-verging thrusts develop as a result of the transmission of shear stress away from an indenting thrust horse block. For instance, the typical triangular zones in the Salt Range (Fig. 1c) developed away from floor thrust blocks propagating into the Salt Range Formation décollement (Baker et al., 1988). A similar setting can be also invoked for the Apennines' examples discussed in Section 4.2. In the Northern Apennines hinterland, the dually-verging thrusts appear to have formed in front, or in-between, basement thrust blocks indenting the basal Burano Fm. décollement (e.g., Finetti et al., 2001). Likewise, in the Southern Apennines fore- and backthrusts developed in the foreland as a result of the forward shearing transmitted by basement thrust blocks (e.g., Menardi Noguera and Rea, 2000).

5. Concluding remarks

Scaled analogue models have been employed to investigate the various styles that can develop in brittle–ductile thrust wedges. The various deformation patterns observed in the models can be qualitatively compared to those described for some natural examples of brittle–ductile thrust wedges. The results of this experimental work suggest the following main conclusions:

(1) different causes or several interrelated factors may contribute to the variability in thrust vergence style (i.e., triangle zones, dominating hinterland/foreland-verging thrusts, passive-roof duplexes). Then, it may be rather difficult to discern the operating factor(s), or dissect the net effect into all of the contributing causes.
(2) the analysis of Type 1 and 1a models has confirmed once more that basal friction can effectively control the structural polarity of brittle–ductile thrust wedges. Very low basal friction favours a σ_1 axis dipping toward the interior of the wedge, hence hinterland-verging thrusting. However, more causes may concur in favouring this style, such as the effect of décollement offset inferred from Type 3 models.
(3) the development of dominating forethrusts and backthrusts in brittle–ductile thrust wedges might be not simply depending on the magnitude of the brittle–ductile coupling (brittle–ductile shear stress ratio), but it could also depend upon the absolute value of décollement strength in relation to brittle overburden strength.
(4) the analysis of the current modelling has revealed a region in the model data point distribution in which there is a clear tendency of backthrusts to deform early forethrusts, a chronology of deformation that has been also identified in natural thrust wedges.
(5) models built with very low basal friction restricted to a strip in front of the model (hybrid Type 1a models) and deformed at relatively slow strain rates are potentially able to trigger diapirism at the core of a long-lived detachment fold. This finding suggests that ductile diapirs can potentially develop in settings dominated exclusively by shortening.
(6) the analysis of Type 2 models suggests the existence of an additional mode of deformation termed "composite-roof duplex", in which both a prograding frontal monocline and outward thrust folding do occur together at mountain fronts. One may speculate that this style is favoured by inadequate erosion above the emergent passive-roof thrust(s).

Acknowledgements

Constructive criticism provided by Prof. H. Koyi and an anonymous reviewer are gratefully acknowledged. Thanks also to Prof. Tom Blenkinsop for editorial assistance. Research supported by CNR – IGG ordinary funds.

References

Allemand, P., 1988. Approche experimentale de la mécanique du rifting continental. Mem. Doc. 38, Cent. Arm. Et. Struct. Socles, Rennes, France. 192 pp.

Anderson, E.M., 1951. The Dynamics of Faulting and Dyke Formation. Olivier and Boyd, Edinburgh.

Baker, D.M., Lillie, R.J., Yeats, R.S., Johnson, G.D., Yousuf, M., Hamid Zamin, A.S., 1988. Development of the Himalayan frontal thrust zone: Salt Range, Pakistan. Geology 16, 3–7.

Baldacci, F., Elter, P., Giannini, E., Giglia, G., Lazzarotto, A., Nardi, R., Tongiorgi, M., 1967. Nuove osservazioni sul problema della Falda Toscana e sulla interpretazione dei flysch arenacei di tipo "Macigno" dell'Appennino Settentrionale. Memorie della Società Geologica Italiana 6, 218–244.

Bally, A.W., Burbi, L., Cooper, C., Ghelardoni, R., 1986. Balanced sections and seismic reflection profiles across the central Apennines. Memorie della Società Geologica Italiana 35, 257–310.

Banks, C.J., Warburton, J., 1986. "Passive-roof" duplex geometry in the frontal structures of the Kirthar and Sulaiman mountain belts, Pakistan. Journal of Structural Geology 8, 229–237.

Barnes, P.M., Nicol, A., 2004. Formation of an active thrusts triangle zone associated with structural inversion in a subduction setting, eastern New Zealand. Tectonics 23, TC1015, doi:10.1029/2002TC001449.

Bello, M., Franchino, A., Merlini, S., 2000. Structural model of Eastern Sicily. Memorie della Società Geologica Italiana 55, 61–70.

Byrne, D.E., Wang, W.H., Davis, D.M., 1993. Mechanical role of backstops in the growth of fore-arcs. Tectonics 12, 123–144.

Bonini, M., 2001. Passive roof thrusting and forelandward fold propagation in scaled brittle–ductile physical models of thrust wedges. Journal of Geophysical Research 106, 2291–2311.

Bonini, M., 2003. Detachment folding, fold amplification, and diapirism in thrust wedge experiments. Tectonics 22, 1065, doi:10.1029/2002TC001458.

Bonini, M., Sani, F., 2002. Extension and compression in the Northern Apennines (Italy) hinterland: evidence from the Late Miocene–Pliocene Siena–Radicofani Basin and relations with basement structures. Tectonics 21, doi:10.1029/2001TC900024.

Brun, J.P., 1999. Narrow rifts versus wide rifts: inferences for the mechanics of rifting from laboratory experiments. Philosophical Transactions of the Royal Society of London 357, 695–712.

Chapple, W.M., 1978. Mechanics of thin-skinned fold-and-thrust belts. Geological Society of America Bulletin 89, 1189–1198.

Cobbold, P.R., Szatmari, P., Demercian, L.S., Coelho, D., Rossello, E.A., 1995. Seismic and experimental evidence for thin-skinned horizontal shortening by convergent radial gliding on evaporites, deep-water Santos

Basin, Brazil. In: Jackson, M.P.A., Roberts, D.G., Snelson, S. (Eds.), Salt Tectonics: A Global Perspective. AAPG Memoir 65, 305–321.

Colletta, B., Letouzey, J., Pinedo, R., Ballard, J.F., Balé, P., 1991. Computerized X-ray tomography analysis of sandbox models: examples of thin-skinned thrust systems. Geology 19, 1063–1067.

Costa, E., Vendeville, B.C., 2001. Diapirism in convergent settings triggered by hinterland pinch-out of viscous decollement: a hypothesis from modeling. In: Koyi, H.A., Mancktelow, N.S. (Eds.), Tectonics Modeling: A Volume in Honor of Hans Ramberg. Geological Society of America Memoir 193, 123–130.

Costa, E., Vendeville, B.C., 2002. Experimental insights on the geometry and kinematics of fold-and-thrust belts above weak, viscous evaporitic décollement. Journal of Structural Geology 24, 1729–1739.

Cotton, J.T., Koyi, K.A., 2000. Modeling of thrust fronts above ductile and frictional detachments: application to structures in the Salt Range and Potwar Plateau, Pakistan. Geological Society of America Bulletin 112, 351–363.

Couzens, B.A., Wiltschko, D.V., 1996. The control of mechanical stratigraphy on the formation of triangle zones. Bulletin of Canadian Petroleum Geology 44, 165–179.

Couzens-Schultz, B.A., Vendeville, B.C., Wiltschko, D.V., 2003. Duplex style and triangle zone formation: insights from physical modeling. Journal of Structural Geology 25, 1623–1644.

Dahlen, F.A., Suppe, J., Davis, D., 1984. Mechanics of fold-and-thrust belts and accretionary wedges: Cohesive Coulomb theory. Journal of Geophysical Research 89, 10087–10101.

Davis, D.M., Engelder, T., 1985. The role of salt in fold-and-thrust belts. Tectonophysics 119, 67–88.

Davis, D.M., Engelder, T., 1987. Thin-skinned deformation over salt. In: Lerche, I., O'Brien, J.J. (Eds.), Dynamical Geology of Salt and Related Structures. Academic Press, San Diego, California, pp. 301–337.

Davis, D.M., Suppe, J., Dahlen, F.A., 1983. Mechanics of fold-and-thrust belts and accretionary wedges. Journal of Geophysical Research 88, 1153–1172.

Davy, P., Cobbold, P.R., 1991. Experiments on shortening of 4-layer model of the continental lithosphere. In: Cobbold, P.R. (Ed.), Experimental and Numerical Modelling of Continental Deformation. Tectonophysics 188, 1–25.

De Feyter, A.J., Menichetti, M., 1986. Back thrusting in forelimbs of rootless anticlines, with examples from the Umbro-Marchean Apennines (Italy). Memorie della Società Geologica Italiana 35, 357–370.

Deng, X., Underwood, M.B., 2001. Abundance of smectite and the location of a plate-boundary fault, Barbados accretionary prism. Geological Society of America Bulletin 113, 495–507.

Dickinson, W.R., Seely, D.R., 1979. Structure and stratigraphy of forearc regions. AAPG Bulletin 63, 2–31.

Doglioni, C., Merlini, S., Cantarella, G., 1999. Foredeep geometries at the front of the Apennines in the Ionian Sea (central Mediterranean). Earth and Planetary Science Letters 168, 243–254.

Elliott, D., 1976. The motion of thrust sheets. Journal of Geophysical Research 81, 949–962.

Ellis, S.M., Schreurs, G., Panien, M., 2004. Comparisons between analogue and numerical models of thrust wedge development. Journal of Structural Geology 26, 1659–1675.

Erickson, S.G., 1995. Mechanics of triangle zones and passive-roof duplexes: implications of finite element models. Tectonophysics 245, 1–11.

Finetti, I., Boccaletti, M., Bonini, M., Del Ben, A., Geletti, R., Pipan, M., Sani, F., 2001. Crustal section based on CROP seismic data across the North Tyrrhenian–Northern Apennines–Adriatic Sea. Tectonophysics 343, 135–163.

Gartrell, A.P., 2001. Crustal rheology and its effect on rift basin styles. In: Koyi, H.A., Mancktelow, N.S. (Eds.), Tectonics Modeling: A Volume in Honor of Hans Ramberg. Geological Society of America Memoir 193, 221–233.

Gordy, P.L., Frey, F.R., Norris, D.K., 1977. Geological Guide for the C.S.P.G. and 1977 Waterton–Glacier Park Field Conference. Canadian Society of Petroleum Geology, Calgary, Alberta, pp. 1–93.

Gutscher, M.A., Kukowski, N., Malavieille, J., Lallemand, S., 1998. Episodic imbricate thrusting and underthrusting: Analog experiments and mechanical analysis applied to the Alaskan Accretionary Wedge. Journal of Geophysical Research 103, 10,161–10,176.

Gutscher, M.A., Klaeschen, D., Flueh, E., Malavieille, J., 2001. Non-Coulomb wedges, wrong-way thrusting, and natural hazards in Cascadia. Geology 29, 379–382.

Harrison, J.C., 1995. Tectonics and kinematics of a foreland folded belt influenced by salt, Arctic Canada. In: Jackson, M.P.A., Roberts, D.G., Snelson, S. (Eds.), Salt Tectonics: A Global Perspective. AAPG Memoir 65, 379–412.

Hafner, W., 1951. Stress distributions and faulting. Geological Society of America Bulletin 62, 373–398.

Hubbert, M.K., 1937. Theory of scale models as applied to the study of geologic structures. Geological Society of America Bulletin 48, 1459–1520.

Jackson, M.P.A., Vendeville, B.C., 1994. Regional extension as a geologic trigger for diapirism. Geological Society of America Bulletin 106, 57–73.

Jamison, W.R., 1996. Mechanical models of triangle zone evolution. Bulletin of Canadian Petroleum Geology 44, 180–194.

Jones, P.B., 1996. Triangle zone geometry, terminology and kinematics. Bulletin of Canadian Petroleum Geology 44, 139–152.

Jouanne, F., Genaudeau, N., Ménard, G., Darmendrail, X., 1998. Estimating present-day displacement fields and tectonic deformation in active mountain belts: an example from the Chartreuse Massif and the southern Jura Mountains, western Alps. Tectonophysics 296, 403–419.

Koyi, H., 1998. The shaping of salt diapirs. Journal of Structural Geology 20, 321–338.

Koyi, H., Sans, M., 2006. Deformation transfer in viscous detachments: comparison of sandbox models to the South Pyrenean Triangle Zone. In: Buiter, S.J.H., Schreurs, G. (Eds.), Analogue and Numerical Modelling of Crustal-Scale Processes. Geological Society of London Special Publication 253, 117–134.

Koyi, H., Hessami, K., Teixell, A., 2000. Epicenter distribution and magnitude of earthquakes in fold-thrust belts: insights from sandbox modelling. Geophysical Research Letters 27, 273–276.

MacKay, M.E., 1995. Structural variation and landward vergence at the toe of the Oregon accretionary prism. Tectonics 14, 1309–1320.

Massoli, D., Koyi, H.A., Barchi, M.R., 2006. Structural evolution of a fold and thrust belt generated by multiple décollements: analogue models and natural examples from the Northern Apennines (Italy). Journal of Structural Geology 28, 185–199.

McKay, M.E., Moore, G.F., Cochrane, G.R., Moore, J.C., Kulm, L.D., 1992. Landward vergence and oblique structural trends in the Oregon margin accretionary prism: implications and effect on fluid flow. Earth and Planetary Science Letters 109, 477–491.

Mackay, P.A., Varsek, J.L., Kubli, T.E., Dechesne, R.G., Newson, A.C., Reid, J.P., 1996. Triangle zones and tectonic wedges: an introduction. Bulletin of Canadian Petroleum Geology 44, 1–5.

Mandl, G., Shippam, G.K., 1981. Mechanical model of thrust sheet gliding and imbrication. In: McClay, K.R., Price, N.J. (Eds.), Thrust and Nappe Tectonics. Geological Society of London Special Publication 9, 79–97.

Menardi Noguera, A., Rea, G., 2000. Deep structure of the Campanian–Lucanian Arc (Southern Apennine, Italy). Tectonophysics 324, 239–265.

Mueller, K., Suppe, J., 1997. Growth of Wheeler Ridge anticline, California: geomorphic evidence for fault-bend folding behaviour during earthquakes. In: Anastasio, D.J., Erslev, E.A., Fisher, D.M., Evans, J.P. (Eds.), Fault-Related Folding. Journal of Structural Geology 19, 383–396.

Mugnier, J.L., Baby, P., Colletta, B., Vinour, P., Bale, P., Leturmy, P., 1997. Thrust geometry controlled by erosion and sedimentation: a view from analogue models. Geology 25, 427–430.

Mulugeta, G., 1988. Modelling the geometry of Coulomb thrust wedges. Journal of Structural Geology 10, 847–859.

Mulugeta, G., Koyi, H., 1987. Three-dimensional geometry and kinematics of experimental piggyback thrusting. Geology 15, 1052–1056.

Nieuwland, D.A., Leutscher, J.H., Gast, J., 2000. Wedge equilibrium in fold-and-thrust belts: prediction of out-of-sequence thrusting based on sandbox experiments and natural examples. Geologie en Mijnbouw 79, 81–91.

Pennock, E.S., Lillie, R.J., Zaman, A.S.H., Yousaf, M., 1989. Structural interpretation of seismic reflection data from Eastern Salt Range and Potwar Plateau, Pakistan. AAPG Bulletin 73, 841–857.

Philippe, Y., 1995. Rampes latérales et zones de transfert dans les chaînes plissées: géométrie, conditions de formation et pièges structuraux associés. Ph.D. thesis, Université de Savoie.

Price, R.A., 1981. The Cordilleran foreland thrust and fold belt in the southern Canadian Rocky Mountains. In: McClay, K.R., Price, N.J. (Eds.), Thrust and Nappe Tectonics. Geological Society of London Special Publication 9, 427–448.

Ramberg, H., 1981. Gravity, Deformation and Earth's Crust. Academic Press, San Diego, Calif, 452 pp.

Smit, J.H.W., Brun, J.P., Sokoutis, D., 2003. Deformation of brittle–ductile thrust wedges in experiments and nature. Journal of Geophysical Research 108. art. no. 2480.

Sommaruga, A., 1999. Décollement tectonics in the Jura foreland fold-and-thrust belt. Marine and Petroleum Geology 16, 111–134.

Stockmal, G., 1983. Modeling of large-scale accretionary wedge deformation. Journal of Geophysical Research 88, 8271–8287.

Salvini, F., Storti, F., McClay, K., 2001. Self-determining numerical modeling of compressional fault-bend folding. Geology 29, 839–842.

Strayer, L.M., Hudleston, P.J., Lorig, L.J., 2001. A numerical model of deformation and fluid-flow in an evolving thrust wedge. Tectonophysics 335, 121–145.

Teyssier, C., 1985. A crustal thrust system in an intracratonic tectonic environment. Journal of Structural Geology 7, 689–700.

Vendeville, B.C., 1991. Thin-skinned compressional structures above frictional plastic and viscous décollement layers. Geological Society of America Abstracts with Programs 23 (5), A423.

Vrolijk, P., 1990. On the mechanical role of smectite in subduction zones. Geology 18, 703–707.

Weijermars, R., 1986. Flow behaviour and physical chemistry of bouncing putties and related polymers in view of tectonic laboratory applications. Tectonophysics 124, 325–358.

Weijermars, R., Schmeling, H., 1986. Scaling of Newtonian and non-Newtonian fluid dynamics without inertia for quantitative modelling of rock flow due to gravity (including the concept of rheological similarity). Physics of the Earth and Planetary Interiors 43, 316–330.

Weijermars, R., Jackson, M.P.A., Vendeville, B., 1993. Rheological and tectonic modeling of salt provinces. Tectonophysics 217, 143–174.

Willett, S., Beaumont, C., Fullsack, P., 1993. A mechanical model for the tectonics of doubly vergent compressional orogens. Geology 21, 371–374.

Wissing, S., Ellis, S., Pfiffner, O.A., 2003. Numerical models of Alpine-type cover nappes. Tectonophysics 367, 145–172.